Incorporating Nuclear Quantum Effects in Molecular Dynamics

Zehua Chen and Yang Yang*

Theoretical Chemistry Institute and Department of Chemistry,

University of Wisconsin-Madison, 1101 University Avenue, Madison, WI 53706, USA

Abstract

The accurate incorporation of nuclear quantum effects in large-scale molecular dynamics simulations remains a significant challenge. Here, we develop a new formulation of the equations of motion of molecular dynamics that incorporates nuclear quantum effects, enabling molecular dynamics simulations to be performed on an effective energy surface obtained from a constrained energy minimization with given quantum nuclear expectation positions. Using a series of model systems, we find that this new approach is significantly more accurate in describing vibrations than classical molecular dynamics and can accurately describe tunneling, which classical molecular dynamics is unable to do. With a lower computational cost, this approach is comparable to or more accurate than centroid molecular dynamics and ring-polymer molecular dynamics.

Nuclear quantum effects (NQEs) [1] have a great impact on the structural, thermodynamical, and kinetic properties of a wide range of chemical and biological systems [2]. They usually include zero-point and tunneling effects and are significant when light nuclei, such as hydrogen, are present. The accurate incorporation of NQEs in molecular simulations is important for understanding many fundamental properties but remains a significant challenge for large-scale molecular simulations. For example, the anomalous properties of water are closely related to the NQEs of the complex hydrogen bond network [3, 4] and thus cannot be fully explained with classical molecular dynamics (MD) without an accurate inclusion of NQEs [5].

There have been many theoretical developments on the incorporation of NQEs in molecular simulations. Some empirical force fields [6] have been used to include NQEs implicitly, and have been able to treat protons and deuteriums differently in water [7]. Quantum wave packet dynamics is based on the exact time evolution of a quantum system according to the time-dependent Schrödinger equation and can give theoretical predictions that accurately match to experiments [8–12]. Quantum trajectory methods [13] are based on the de Broglie-Bohm formulation of quantum mechanics [14–18], which attributes all quantum effects to the quantum potential. With a reasonable approximation to the quantum potential, quantum trajectory methods have been applied to many model systems and give accurate results [19, 20]. Multicomponent quantum theories [21–26] also include NQEs in real-time simulations [27–31]. They usually simultaneously treat both electrons and key nuclei quantum mechanically and therefore do not rely on conventional Born-Oppenheimer potential energy

surfaces (PESs). Dynamics simulations can be performed through quantum time evolution of multicomponent wave functions or density matrices [29, 30], and practical problems, such as proton transfer processes, have been studied with multicomponent quantum theory [32].

Although the aforementioned methods are highly accurate in describing NQEs, they are often hindered by their high computational costs in large molecular or bulk systems. This challenge can be partially addressed using methods based on the path integral formulation of quantum mechanics [33, 34]. By simultaneously simulating a set of coupled replicas for a system, path integral molecular dynamics (PIMD) [35, 36] is able to capture NQEs and accurately describe many static properties of the system [37]. Its extensions such as ring-polymer molecular dynamics (RPMD) [38] and centroid molecular dynamics (CMD) [39–44] can describe dynamical properties using approximate correlation functions. While dynamical properties from RPMD and CMD are considerably more accurate than those from classical MD, challenges still exist with spurious frequencies in RPMD and curvature problems in CMD. Both of these problems can lead to unreliable vibrational spectra [45], although several recent developments can mitigate them to some extent, including thermostatted RPMD [46, 47], Matsubara dynamics [48], and quasicentroid molecular dynamics [49].

In this Letter, we present an alternative formulation for the equations of motion of classical MD that incorporates NQEs. With this new formulation, NQEs can be efficiently and accurately described with MD on an effective PES, which in practice is approximated by a constrained minimized energy surface (CMES). We first analytically show that CMES-MD remains exact for the harmonic oscillator model. Then, with numerical analyses of a Morse oscillator model and a quartic double-well potential model, we show that CMES-MD is generally much more accurate in describing vibrations and tunneling effects than conventional MD, RPMD, and CMD.

We start with the polar representation of a time-dependent wave function $\psi(\boldsymbol{x}, t) = A(\boldsymbol{x}, t) \exp(\mathrm{i}S(\boldsymbol{x}, t)/\hbar)$, where the amplitude A and the phase S are both real functions. For simplicity, we assume that there is only one quantum particle throughout our derivation. However, the formulation can be easily generalized to multiple quantum particle cases if the particles can be assumed to be distinguishable, such as nuclei in regular molecular and bulk systems. With this polar representation, the kinetic energy can be decomposed into two

terms

$$\langle\hat{T}\rangle(t) = \int \mathrm{d}\boldsymbol{x} A(\boldsymbol{x},t)\frac{(-\mathrm{i}\hbar\nabla)^2}{2m}A(\boldsymbol{x},t) + \frac{1}{2m}\int \mathrm{d}\boldsymbol{x} A^2(\boldsymbol{x},t)[\nabla S(\boldsymbol{x},t)]^2. \tag{1}$$

The first term is the kinetic energy evaluated with the amplitude function A only. Since A is associated with the real space probability density distribution with $\rho(\boldsymbol{x},t) = A^2(\boldsymbol{x},t)$, this term can be perceived as the kinetic energy due to quantum delocalization, or the zero-point kinetic energy. In the second term, the key quantity ∇S is associated with the observable momentum and is in fact the momentum field in Bohmian mechanics [14–18] with the definition $\boldsymbol{p}(\boldsymbol{x},t) = \nabla S(\boldsymbol{x},t)$. Therefore, after multiplying $[\nabla S(\boldsymbol{x},t)]^2/2m$ with the probability density $A^2(\boldsymbol{x},t)$ and integrating over the spatial variable, the second term can be considered as the kinetic energy associated with the observable momentum $\boldsymbol{p}$.

With the variance of the observable momentum defined as the variance of the momentum field in Bohmian mechanics:

$$\sigma_{\boldsymbol{p}}^2(t) \equiv \int \mathrm{d}\boldsymbol{x} A^2(\boldsymbol{x},t)[\nabla S(\boldsymbol{x},t)]^2 - \langle\boldsymbol{p}\rangle^2(t), \tag{2}$$

the kinetic energy can be further expressed as

$$\langle\hat{T}\rangle(t) = \langle A(t)|\hat{T}|A(t)\rangle + \frac{\langle\hat{\boldsymbol{p}}\rangle^2(t)}{2m} + \frac{\sigma_{\boldsymbol{p}}^2(t)}{2m}. \tag{3}$$

The terms in Eq. 3 correspond to, respectively, the zero-point kinetic energy, the classical kinetic energy associated with the expectation value of the observable momentum, and an energy contribution from the variance of the observable momentum.

Another way of expressing the kinetic energy is simply $\langle\hat{T}\rangle(t) = \langle\hat{H}\rangle(t) - \langle\hat{V}\rangle(t)$, which can be plugged into the left side of Eq. 3. Then we can take the time derivative on both sides of the equation and simplify the equation into

$$\frac{\langle\hat{\boldsymbol{p}}\rangle}{m}\cdot\frac{\mathrm{d}\langle\hat{\boldsymbol{p}}\rangle}{\mathrm{d}t} = \left\langle\frac{\partial V}{\partial t}\right\rangle - \frac{\mathrm{d}}{\mathrm{d}t}\langle A(t)|\hat{H}(t)|A(t)\rangle - \frac{\mathrm{d}}{\mathrm{d}t}\frac{\sigma_{\boldsymbol{p}}^2}{2m}. \tag{4}$$

Note that we have used the relationship $\mathrm{d}\langle\hat{H}\rangle(t)/\,\mathrm{d}t = \langle\partial V/\partial t\rangle$ in the simplification procedure. Eq. 4 relates the time dependence of momentum to the time dependence of energetic terms. It is exact without any approximation. However, in order to make it into an equation of motion that can be practically used, we next proceed with two major approximations.

First, we neglect the derivative of the momentum variance term, which is generally hard to evaluate. Second, we invoke an adiabatic approximation and assume that the quantum state $|A\rangle$ does not explicitly depend on time. This is done by a constrained minimization, where we assume that the wave function of the quantum particle can adapt to the energy-minimized quantum state at a particular expectation position during the dynamics process. Therefore, the wave function only explicitly depends on the expectation position rather than time. We note that these two approximations are not trivially justifiable, and their applicability as well as limitations will be discussed later in this Letter. With the second approximation, the quantum state $|A\rangle$ can be obtained from a constrained minimization for the total energy with the following Lagrangian:

$$\mathcal{L} = \langle A|\hat{H}(t)|A\rangle + \boldsymbol{f}\cdot(\langle A|\hat{\boldsymbol{x}}|A\rangle - \langle\hat{\boldsymbol{x}}\rangle(t)) - \tilde{E}(\langle A|A\rangle - 1), \tag{5}$$

where $\boldsymbol{f}$ is the Lagrange multiplier associated with the expectation position constraint, $\tilde{E}$ is the Lagrange multiplier associated with the wave function normalization constraint, and $\langle\hat{\boldsymbol{x}}\rangle(t)$ is the expectation position at time t. Making the Lagrangian function stationary under the expectation position constraint and the normalization constraint leads to the eigenvalue equation:

$$[\hat{H}(t) + \boldsymbol{f}\cdot\hat{\boldsymbol{x}}]|A\rangle = \tilde{E}|A\rangle, \tag{6}$$

where $|A\rangle$ is the eigenstate, the Lagrange multiplier $\tilde{E}$ is the associated eigenvalue, and $\boldsymbol{f}$ needs be solved iteratively so that $|A\rangle$ satisfies the constraints.

With both approximations applied and the quantum state $|A\rangle$ obtained as a function of $\langle\hat{\boldsymbol{x}}\rangle(t)$, we can simplify Eq. 4 into

$$\frac{\langle\hat{\boldsymbol{p}}\rangle}{m}\cdot\frac{\mathrm{d}\langle\hat{\boldsymbol{p}}\rangle}{\mathrm{d}t} \approx -\left\langle\frac{\mathrm{d}A}{\mathrm{d}t}\middle|\hat{H}(t)\middle|A\right\rangle - \left\langle A\middle|\hat{H}(t)\middle|\frac{\mathrm{d}A}{\mathrm{d}t}\right\rangle \tag{7}$$

$$= -\frac{\mathrm{d}\langle\hat{\boldsymbol{x}}\rangle}{\mathrm{d}t}\cdot\Big[\langle\nabla_{\langle\hat{\boldsymbol{x}}\rangle}A|\hat{H}(t)|A\rangle + \langle A|\hat{H}(t)|\nabla_{\langle\hat{\boldsymbol{x}}\rangle}A\rangle\Big] \tag{8}$$

$$= -\frac{\langle\hat{\boldsymbol{p}}\rangle}{m}\cdot\nabla_{\langle\hat{\boldsymbol{x}}\rangle}\langle A|\hat{H}(t)|A\rangle. \tag{9}$$

Note that here we have used the Ehrenfest theorem $\mathrm{d}\langle\hat{\boldsymbol{x}}\rangle/\,\mathrm{d}t = \langle\hat{\boldsymbol{p}}\rangle/m$. Since it is reasonable to assume that the change of $\langle\hat{\boldsymbol{p}}\rangle$ should have an opposite direction to the energy gradient term $(\nabla_{\langle\hat{\boldsymbol{x}}\rangle}\langle A|\hat{H}(t)|A\rangle)$, the common prefactor $|\langle\hat{\boldsymbol{p}}\rangle|/m$ can be dropped and we arrive at the

final expression

$$\frac{\mathrm{d}\langle\hat{\boldsymbol{p}}\rangle}{\mathrm{d}t} \approx -\nabla_{\langle\hat{\boldsymbol{x}}\rangle}\langle A|\hat{H}(t)|A\rangle \equiv -\nabla_{\langle\hat{\boldsymbol{x}}\rangle}V^{\mathrm{CMES}}(\langle\hat{\boldsymbol{x}}\rangle), \tag{10}$$

where V^{CMES} is the constrained minimized energy surface (CMES). Together with $\mathrm{d}\langle\hat{\boldsymbol{x}}\rangle/\,\mathrm{d}t = \langle\hat{\boldsymbol{p}}\rangle/m$, they form the equations of motion for CMES-MD. These equations of motion represent a new way of performing MD simulations that explicitly include NQEs. They are highly similar in structure to Newton's equations used in conventional MD simulations, with the difference that the time evolution is now on the quantum expectation positions and momenta rather than the classical ones. Furthermore, V^{CMES} is the energy associated with the quantum state $|A\rangle$ rather than the classical potential, and consequently, quantum effects are inherently incorporated in CMES-MD based on V^{CMES}.

In this Letter, we investigate the model systems of a harmonic oscillator, a Morse oscillator and a quartic double-well potential, which have easily accessible exact quantum solutions and can be compared with RPMD and CMD at a reasonable computational cost. For the Morse oscillator and the quartic double-well models, classical MD and CMES-MD are performed with an in-house python script, and 1-dimensional RPMD and CMD simulations are performed with a modified i-PI package [50]. The computational details are described in the Supplemental Material. We note that in principle, CMES-MD can also be applied to molecular systems, and current research in our group is being pursued using the energy surface from constrained nuclear-electronic orbital density functional theory (cNEO-DFT) [51, 52] as an approximation to the CMES.

The 1-dimensional harmonic oscillator $\hat{H} = \hat{p}^2/2m + m\omega^2\left(\hat{x} - x_{\mathrm{e}}\right)^2/2$ is one particular model for which classical MD gives the same trajectory as the exact quantum theory. RPMD and CMD are also exact for this model system. For CMES-MD, since $\hat{H} + f\hat{x}$ represents the harmonic oscillator with shifted energy and shifted position based on the value of f, the constrained minimized energy state $|A\rangle$ for any expectation position $\langle\hat{x}\rangle$ is the ground state wave function of $\hat{H}$ shifted to the expectation position $\langle\hat{x}\rangle$. Finally, the corresponding energy surface as a function of the expectation position $\langle\hat{x}\rangle$ is

$$V^{\mathrm{CMES}}(\langle\hat{x}\rangle) = \frac{\hbar\omega}{2} + \frac{1}{2}m\omega^2\left(\langle\hat{x}\rangle - x_{\mathrm{e}}\right)^2. \tag{11}$$

This effective potential universally shifts the original harmonic potential upwards by $\hbar\omega/2$, which is the well-known zero-point energy for a harmonic oscillator (see Fig. S1). This result may seem counterintuitive since conventionally ZPE is considered to be a property

of the whole energy surface rather than a point-wise property, however, we note that here the ZPE should be more accurately considered as a quantum delocalization energy, which always exists as the quantum wave packet travels in the space. Since classical MD produces the exact trajectory on the harmonic potential, the trajectory produced by CMES-MD on V^{CMES} will also be exact without any need for numerical tests.

Compared with the harmonic oscillator, the Morse potential is a better model for chemical bonds with anharmonic effects. Here we use a Morse potential that can mimic the stretch of the O−H bond and perform simulations using classical MD, CMES-MD, RPMD, and CMD. In CMES-MD, the CMES is solved numerically on grids with the finite difference method and its numerical gradient is then used as the force according to Eq. 10. The exact quantum results are used as references, which are obtained from the analytical solution of the Morse potential.

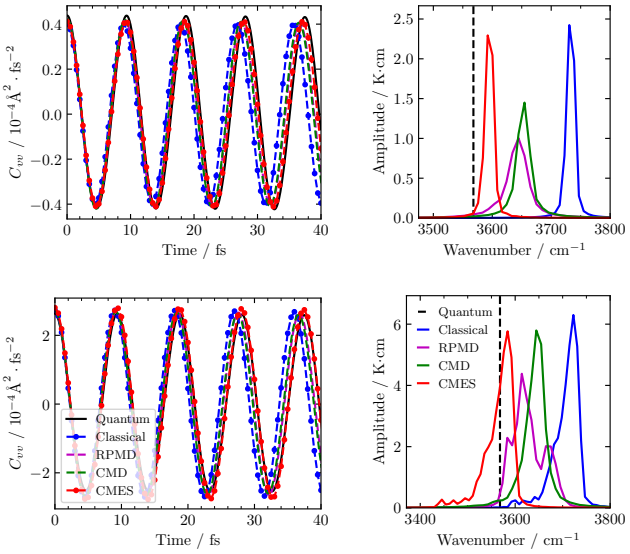

FIG. 1. Velocity autocorrelation functions C_{vv} and power spectra of the Morse oscillator at 50 K (upper) and 300 K (lower). The potential form is $V(x) = D_{\mathrm{e}}(\mathrm{e}^{-2\alpha(x-x_{\mathrm{e}})} - 2\mathrm{e}^{-\alpha(x-x_{\mathrm{e}})})$, where $D_{\mathrm{e}} = hc\omega_{\mathrm{e}}^2/4\omega_{\mathrm{e}}\chi_{\mathrm{e}}$ and $\alpha = \sqrt{2\mu hc\omega_{\mathrm{e}}\chi_{\mathrm{e}}/\hbar^2}$ with the reduced mass taken from molecule $^{16}\mathrm{O}^{1}\mathrm{H}$. ALl the parameters are the same as those used in Ref. 46, with $\omega_{\mathrm{e}} = 3737.76\,\mathrm{cm}^{-1}$, $\omega_{\mathrm{e}}\chi_{\mathrm{e}} = 84.881\,\mathrm{cm}^{-1}$, and $x_{\mathrm{e}} = 0.96966\,\text{Å}$. The dashed vertical line represents the exact quantum frequency $3568\,\mathrm{cm}^{-1}$.

Fig. 1 shows the velocity autocorrelation functions and the corresponding power spectra of classical MD, CMES-MD, RPMD, and CMD at two different temperatures, along with the exact quantum references. Compared with the Kubo-transformed quantum velocity auto-

correlation function [53], classical MD underestimates the period of the correlation function and therefore severely overestimates the vibrational frequency. RPMD and CMD can more accurately describe the correlation function and their overestimations of the vibrational frequencies are significantly less than those of classical MD. CMES-MD is noticeably more accurate than RPMD and CMD with better agreement with the exact quantum correlation functions and more accurate vibrational frequencies. Note that conventionally RPMD and CMD are known to have problems in describing molecular vibrations with spurious frequencies for RPMD and curvature problems for CMD. However, these problems did not show up in this simple one-dimensional one-mode model system. Despite this fact, CMES-MD still outperforms these methods in terms of both accuracy and efficiency. These results suggest that with a low computational cost that is only slightly higher than that of classical MD, CMES-MD can accurately describe bond vibrations that are highly anharmonic.

As the temperature increases, CMES-MD and other simulation methods start to have broader vibrational peaks. This peak broadening is accompanied by a red shift in the peak position as a result of the anharmonic potential energy surface. For this Morse potential, we observe that for a temperature between 50 K and 1500 K (see Fig. S2), CMES-MD is always the most accurate among all the methods we tested.

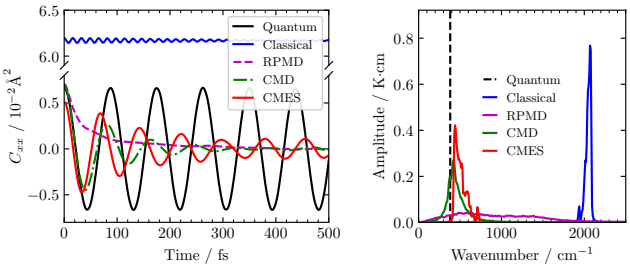

FIG. 2. Position autocorrelation function C_{xx} and power spectrum of the double-well potential at 50 K. The potential form is $V(x) = ax^2 + bx^4$, where $a = -4\,\mathrm{eV/Å}^2$ and $b = 32\,\mathrm{eV/Å}^4$. The mass of the particle is the same as the mass of a proton. The dashed vertical line represents the exact quantum frequency 382 cm^{-1}.

Next we investigate a more challenging double-well potential model, in which quantum tunneling is expected to occur. We use a quartic double-well potential with a 0.125 eV barrier height and a 0.5 Å separation between the potential minima, which can roughly represent the potential energy landscape for a practical proton transfer reaction. The CMES and

its gradients for the quartic double-well potential are determined via the same procedure as is used for the Morse potential, solving numerically on grids with the finite difference method. As shown in Fig. S3, the CMES of this double-well potential is a single well with the minimum located at $\langle \hat{x} \rangle = 0$. This huge difference between the original potential and the effective potential may initially seem counterintuitive. In fact, it is the key to the success of CMES-MD and can be understood in the following way: the ground state for this double-well potential has a symmetrical wave function with two peaks, whose expectation position is at $\langle \hat{x} \rangle = 0$. Therefore, the CMES has its minimum at $\langle \hat{x} \rangle = 0$. As the constrained expectation position deviates from the center, the constrained minimized wave function becomes less symmetrical with more and more excited state characters mixed in, thus increasing the energy and forming a single-well effective potential. On this single-well effective potential, the quantum expectation position moves smoothly between left and right as if the barrier does not exist, which is in agreement with the quantum picture, where the wave function can tunnel through the barrier back and forth with a smooth oscillation for the quantum expectation position. This physical picture can be quantitatively verified by the agreement between the tunneling frequency by CMES-MD and the exact quantum tunneling frequency as shown in Fig. 2. In contrast, classical MD completely fails in predicting this tunneling effect with almost all simulations at low temperatures trapped in local minima of the double-well. Therefore, classical MD gives position autocorrelation functions that are not vertically centered at zero, and its vibrational frequency is close to the Hessian value around the local minimum, which is about 5 times larger than the quantum tunneling frequency. Unlike in the Morse oscillator case, the two path-integral methods show significant differences in the double-well potential model, as CMD gives good autocorrelation functions and predicts a relatively sharp peak with an accurate tunneling frequency, whereas RPMD suffers from a fast decay of the correlation function and a broad peak that smears over a range of nearly $2000\,\mathrm{cm}^{-1}$. As the temperature increases, classical MD starts to have redshifts in the peak positions, and CMES-MD and CMD see blueshifts. At 1500 K, all simulation methods behave very similarly with broad peaks that maximize around 1300-1500 cm^{-1} (see Fig. S4). All of these results from CMES-MD show that CMES-MD is comparable to the accurate CMD method in describing the dynamics in the double-well potential system, but at a much lower computational cost.

The good performance of CMES-MD suggests that the approximations that we made

during the derivations are reasonable. These approximations mainly include the neglect of the change of the momentum variance and the adiabatic approximation that assumes that the quantum particle can adapt its wave function distribution to the lowest-energy state on a time scale that is faster than its spatial movement. However, we note that it is possible that in some circumstances these approximations may break down and CMES-MD may fail. For example, if significant reflection exists in the process, the time derivative of the momentum variance may not be negligible, and when the particle is moving very fast, the probability distribution may not adapt fast enough to the constrained minimized wave function, thus breaking the adiabatic approximation. In addition, similarly to conventional MD, the classical treatment brings not only efficiency but also some limitations. For example, quantum coherence is missing, which is reflected by a decreasing amplitude of the correlation function, and heat capacities will not approach zero when $T \to 0\,\mathrm{K}$ due to the loss of the energy quantization picture. Furthermore, classical dynamics with distinguishable particles is incapable of capturing the exchange effect, which is important in systems with heavily packed particles, such as in a Bose-Einstein condensate [54, 55]. Although detailed studies of these approximations and possible limitations are beyond the scope of the current work, they are important topics for our future research for better understanding the applicabilities and limitations of CMES-MD. We finally note that due to the similarity between CMES-MD and classical MD, we can expect analytical force field models or even machine-learning force fields (ML-FFs) [56] to be built based on the CMES, which will allow for an even more efficient incorporation of NQEs in MD simulations.

In summary, we provide a formal derivation for incorporating NQEs in the framework of MD. This is achieved through the calculation of a CMES, which serves as the effective potential for MD simulations. In CMES-MD, quantum delocalization and tunneling effects are inherently included and therefore CMES-MD is capable of accurately describing dynamical vibrational frequencies that are comparable to or better than CMD and RPMD. Furthermore, CMES-MD is vastly more computationally efficient than conventional ways of including NQEs and can be further accelerated when combined with modern machine-learning techniques in the future. It is a promising method to describe NQEs in larger and more complex systems, which will open the door to broader applications.

We are grateful for the support and funding from the University of Wisconsin via the Wisconsin Alumni Research Foundation. We also thank Dr. Xi Xu and Mr. James Langford

for helpful comments.

* yyang222@wisc.edu

[1] T. E. Markland and M. Ceriotti, Nuclear quantum effects enter the mainstream, Nat Rev Chem **2**, 1 (2018).

[2] L. Pereyaslavets, I. Kurnikov, G. Kamath, O. Butin, A. Illarionov, I. Leontyev, M. Olevanov, M. Levitt, R. D. Kornberg, and B. Fain, On the importance of accounting for nuclear quantum effects in ab initio calibrated force fields in biological simulations, PNAS **115**, 8878 (2018).

[3] A. Nilsson and L. G. M. Pettersson, The structural origin of anomalous properties of liquid water, Nat Commun **6**, 8998 (2015).

[4] M. Ceriotti, W. Fang, P. G. Kusalik, R. H. McKenzie, A. Michaelides, M. A. Morales, and T. E. Markland, Nuclear Quantum Effects in Water and Aqueous Systems: Experiment, Theory, and Current Challenges, Chem. Rev. **116**, 7529 (2016).

[5] L. Zhang, H. Wang, R. Car, and W. E, Phase Diagram of a Deep Potential Water Model, Phys. Rev. Lett. **126**, 236001 (2021).

[6] J. R. Grigera, An effective pair potential for heavy water, J. Chem. Phys. **114**, 8064 (2001).

[7] N. Ben Abu, P. E. Mason, H. Klein, N. Dubovski, Y. Ben Shoshan-Galeczki, E. Malach, V. Pražienková, L. Maletínská, C. Tempra, V. C. Chamorro, J. Cvačka, M. Behrens, M. Y. Niv, and P. Jungwirth, Sweet taste of heavy water, Commun Biol **4**, 1 (2021).

[8] H. D. Meyer, U. Manthe, and L. S. Cederbaum, The multi-configurational time-dependent Hartree approach, Chemical Physics Letters **165**, 73 (1990).

[9] Y. Sun, D. J. Kouri, D. G. Truhlar, and D. W. Schwenke, Dynamical basis sets for algebraic variational calculations in quantum-mechanical scattering theory, Phys. Rev. A **41**, 4857 (1990).

[10] M. H. Alexander, D. E. Manolopoulos, and H.-J. Werner, An investigation of the F+H2 reaction based on a full ab initio description of the open-shell character of the F(2P) atom, J. Chem. Phys. **113**, 11084 (2000).

[11] D. G. Fleming, D. J. Arseneau, O. Sukhorukov, J. H. Brewer, S. L. Mielke, G. C. Schatz, B. C. Garrett, K. A. Peterson, and D. G. Truhlar, Kinetic Isotope Effects for the Reactions of Muonic Helium and Muonium with H2, Science **331**, 448 (2011).

[12] W. Chen, R. Wang, D. Yuan, H. Zhao, C. Luo, Y. Tan, S. Li, D. H. Zhang, X. Wang, Z. Sun, and X. Yang, Quantum interference between spin-orbit split partial waves in the F + HD → HF + D reaction, Science **371**, 936 (2021).

[13] C. L. Lopreore and R. E. Wyatt, Quantum Wave Packet Dynamics with Trajectories, Phys. Rev. Lett. **82**, 5190 (1999).

[14] L. De Broglie, Sur la possibilité de relier les phénomenes d'interférence et de diffractiona la théorie des quanta de lumiere, Comptes Rendus **183**, 447 (1926).

[15] L. De Broglie, La structure atomique de la matière et du rayonnement et la mécanique ondulatoire, CR Acad. Sci. Paris **184**, 273 (1927).

[16] E. Madelung, Quantentheorie in hydrodynamischer Form, Z. Physik **40**, 322 (1927).

[17] D. Bohm, A Suggested Interpretation of the Quantum Theory in Terms of "Hidden" Variables. I, Phys. Rev. **85**, 166 (1952).

[18] D. Bohm, A Suggested Interpretation of the Quantum Theory in Terms of "Hidden" Variables. II, Phys. Rev. **85**, 180 (1952).

[19] S. Garashchuk and V. A. Rassolov, Quantum dynamics with Bohmian trajectories: Energy conserving approximation to the quantum potential, Chemical Physics Letters **376**, 358 (2003).

[20] S. Garashchuk and V. Rassolov, Energy conserving approximations to the quantum potential: Dynamics with linearized quantum force, J. Chem. Phys. **120**, 1181 (2004).

[21] I. L. Thomas, Protonic Structure of Molecules. I. Ammonia Molecules, Phys. Rev. **185**, 90 (1969).

[22] J. F. Capitani, R. F. Nalewajski, and R. G. Parr, Non-Born–Oppenheimer density functional theory of molecular systems, J. Chem. Phys. **76**, 568 (1982).

[23] T. Kreibich and E. K. U. Gross, Multicomponent Density-Functional Theory for Electrons and Nuclei, Phys. Rev. Lett. **86**, 2984 (2001).

[24] S. P. Webb, T. Iordanov, and S. Hammes-Schiffer, Multiconfigurational nuclear-electronic orbital approach: Incorporation of nuclear quantum effects in electronic structure calculations, J. Chem. Phys. **117**, 4106 (2002).

[25] T. Ishimoto, M. Tachikawa, and U. Nagashima, Review of multicomponent molecular orbital method for direct treatment of nuclear quantum effect, Int. J. Quantum Chem. **109**, 2677 (2009).

[26] F. Pavošević, T. Culpitt, and S. Hammes-Schiffer, Multicomponent Quantum Chemistry: Integrating Electronic and Nuclear Quantum Effects via the Nuclear–Electronic Orbital Method, Chem. Rev. **120**, 4222 (2020).

[27] A. Abedi, N. T. Maitra, and E. K. U. Gross, Exact Factorization of the Time-Dependent Electron-Nuclear Wave Function, Phys. Rev. Lett. **105**, 123002 (2010).

[28] Y. Suzuki, A. Abedi, N. T. Maitra, and E. K. U. Gross, Laser-induced electron localization in H 2 + : Mixed quantum-classical dynamics based on the exact time-dependent potential energy surface, Phys. Chem. Chem. Phys. **17**, 29271 (2015).

[29] L. Zhao, Z. Tao, F. Pavošević, A. Wildman, S. Hammes-Schiffer, and X. Li, Real-Time Time-Dependent Nuclear-Electronic Orbital Approach: Dynamics beyond the Born–Oppenheimer Approximation, J. Phys. Chem. Lett. **11**, 4052 (2020).

[30] L. Zhao, A. Wildman, Z. Tao, P. Schneider, S. Hammes-Schiffer, and X. Li, Nuclear–electronic orbital Ehrenfest dynamics, J. Chem. Phys. **153**, 224111 (2020).

[31] Z. Tao, Q. Yu, S. Roy, and S. Hammes-Schiffer, Direct Dynamics with Nuclear–Electronic Orbital Density Functional Theory, Acc. Chem. Res. 10/gnbk32 (2021).

[32] L. Zhao, A. Wildman, F. Pavošević, J. C. Tully, S. Hammes-Schiffer, and X. Li, Excited State Intramolecular Proton Transfer with Nuclear-Electronic Orbital Ehrenfest Dynamics, J. Phys. Chem. Lett. **12**, 3497 (2021).

[33] R. P. Feynman, A. R. Hibbs, and D. F. Styer, *Quantum Mechanics and Path Integrals* (Courier Corporation, 2010).

[34] R. Feynman, Statistical mechanics (redwood city, ca) (1972).

[35] B. J. Berne, G. Ciccotti, and D. F. Coker, *Classical And Quantum Dynamics In Condensed Phase Simulations: Proceedings Of The International School Of Physics* (World Scientific, 1998).

[36] M. E. Tuckerman, Path integration via molecular dynamics, Quantum Simulations of Complex Many-Body Systems: From Theory to Algorithms **10**, 269 (2002).

[37] C. P. Herrero and R. Ramírez, Path-integral simulation of solids, J. Phys.: Condens. Matter **26**, 233201 (2014).

[38] I. R. Craig and D. E. Manolopoulos, Quantum statistics and classical mechanics: Real time correlation functions from ring polymer molecular dynamics, J. Chem. Phys. **121**, 3368 (2004).

[39] J. Cao and G. A. Voth, A new perspective on quantum time correlation functions, J. Chem.

Phys. **99**, 10070 (1993).

[40] J. Cao and G. A. Voth, The formulation of quantum statistical mechanics based on the Feynman path centroid density. I. Equilibrium properties, J. Chem. Phys. **100**, 5093 (1994).

[41] J. Cao and G. A. Voth, The formulation of quantum statistical mechanics based on the Feynman path centroid density. II. Dynamical properties, J. Chem. Phys. **100**, 5106 (1994).

[42] J. Cao and G. A. Voth, The formulation of quantum statistical mechanics based on the Feynman path centroid density. III. Phase space formalism and analysis of centroid molecular dynamics, J. Chem. Phys. **101**, 6157 (1994).

[43] J. Cao and G. A. Voth, The formulation of quantum statistical mechanics based on the Feynman path centroid density. IV. Algorithms for centroid molecular dynamics, J. Chem. Phys. **101**, 6168 (1994).

[44] S. Jang and G. A. Voth, Path integral centroid variables and the formulation of their exact real time dynamics, J. Chem. Phys. **111**, 2357 (1999).

[45] A. Witt, S. D. Ivanov, M. Shiga, H. Forbert, and D. Marx, On the applicability of centroid and ring polymer path integral molecular dynamics for vibrational spectroscopy, J. Chem. Phys. **130**, 194510 (2009).

[46] M. Rossi, M. Ceriotti, and D. E. Manolopoulos, How to remove the spurious resonances from ring polymer molecular dynamics, J. Chem. Phys. **140**, 234116 (2014).

[47] M. Rossi, V. Kapil, and M. Ceriotti, Fine tuning classical and quantum molecular dynamics using a generalized Langevin equation, J. Chem. Phys. **148**, 102301 (2018).

[48] T. J. H. Hele, M. J. Willatt, A. Muolo, and S. C. Althorpe, Boltzmann-conserving classical dynamics in quantum time-correlation functions: "Matsubara dynamics", J. Chem. Phys. **142**, 134103 (2015).

[49] C. Haggard, V. G. Sadhasivam, G. Trenins, and S. C. Althorpe, Testing the quasicentroid molecular dynamics method on gas-phase ammonia, J. Chem. Phys. **155**, 174120 (2021).

[50] M. Ceriotti, J. More, and D. E. Manolopoulos, I-PI: A Python interface for ab initio path integral molecular dynamics simulations, Computer Physics Communications **185**, 1019 (2014).

[51] X. Xu and Y. Yang, Full-quantum descriptions of molecular systems from constrained nuclear–electronic orbital density functional theory, J. Chem. Phys. **153**, 074106 (2020).

[52] X. Xu and Y. Yang, Constrained nuclear-electronic orbital density functional theory: Energy surfaces with nuclear quantum effects, J. Chem. Phys. **152**, 084107 (2020).

[53] R. Kubo, Statistical-Mechanical Theory of Irreversible Processes. I. General Theory and Simple Applications to Magnetic and Conduction Problems, J. Phys. Soc. Jpn. **12**, 570 (1957).

[54] A. Einstein, Quantentheorie des einatomigen idealen Gases. Zweite Abhandlung, in *Albert Einstein: Akademie-Vorträge* (John Wiley & Sons, Ltd, 2005) pp. 245–257.

[55] Bose, Plancks Gesetz und Lichtquantenhypothese, Z. Physik **26**, 178 (1924).

[56] O. T. Unke, S. Chmiela, H. E. Sauceda, M. Gastegger, I. Poltavsky, K. T. Schütt, A. Tkatchenko, and K.-R. Müller, Machine Learning Force Fields, Chem. Rev. **121**, 10142 (2021).